Progress In Electromagnetics Research C, Vol. 122, 243–252, 2022

Fast Computing Method and Response Characteristic Analysis for Array Dielectric Logging

Lianyun Cai[1, 2] and Shaogui Deng[1, 2, *]

Abstract—Dielectric logging is a valuable tool for locating and developing tight reservoirs, low contrast reservoirs, shale oil and gas reservoirs, and other unconventional oil and gas reservoirs. The processing of multi-frequency and multi-spacing dielectric logging measurements is based on a stable and efficient response computation algorithm. An equivalent computation model for the push-against-hole array dielectric logging tool is established in this paper, and an improved forward method based on the semi-analytical algorithm for dielectric logging response is devised. Thus the calculation speed of each measurement point's dielectric logging response is increased by more than 8 times. Dielectric logging response charts are also constructed, showing amplitude attenuation and phase shift as functions of formation resistivity and relative permittivity at various operating frequencies. The effects of mud cake, invasion, and anisotropy on the response signal are then simulated and evaluated. The findings reveal that: (1) as the high-frequency response changes significantly when the mud cake is thick, to correct the mud cake's influence, the mud cake parameters can be extracted using the high-frequency detection mode. (2) Invasion has a complicated effect on the high-frequency response, and higher resistivity or relative permittivity in the invasion zone can readily lead to an oscillatory nonlinear shift in the response as a function of invasion depth. This means that for high-resistivity and high-permittivity formations, high-frequency response has a larger sensitivity and a deeper depth of investigation. (3) When the anisotropy coefficient is small, the high-frequency response is preferable for extracting anisotropy; however, as anisotropy increases, the low-frequency response becomes more sensitive to anisotropy than the high-frequency response.

1. INTRODUCTION

Dielectric logging is a crucial tool for finding and developing unconventional oil and gas reservoirs such as tight oil and gas, heavy oil, and carbonate rock [3, 7, 8]. It works at a high frequency with a short source spacing, necessitates high instrument measurement accuracy, and is heavily influenced by ambient conditions. Because early dielectric logging equipment operates at a single high frequency (1 GHz or above), precise reflection on formation information cannot be guaranteed. The Schlumberger Array Dielectric Logging Tool (ADT) [4], also known as the Dielectric Scanner, and the Baker Hughes, GE (BHGE) company's Array Dielectric eXplorer Formation Evaluation Service [2] both use multi-frequency multi-spacing measurements for formation detection, and the depth of investigation (DOI) can go up to 10 cm, with a resolution of 1 inch (0.0254 cm). They can be used to investigate the properties of formation rock fluids, as well as the dielectric dispersion effect of rock skeletons, and to discern between different geological structures [12–14, 18].

The tool pad is against the borehole wall when this type of tool is in operation. It is a three-dimensional (3D) geological model that includes antennae, a wellbore, and formation. To model the

Received 6 June 2022, Accepted 20 July 2022, Scheduled 13 August 2022

* Corresponding author: Shaogui Deng (dengshg@upc.edu.cn).

[1] School of Geosciences, China University of Petroleum (East China), Qingdao 266580, China. [2] Key Laboratory of Deep Oil and Gas Geology and Exploration, China University of Petroleum (East China), Qingdao 266580, China.

response, 3D numerical methods such as the finite element method and finite-difference approach are commonly utilized. [9] simulated the amplitude attenuation and phase shift of a full-scale dielectric logging tool model based on COMSOL. The effects of mud cake and invasion on the response were simulated, and the sensitivity of the response to formation parameters (resistivity, permittivity, dip angle, anisotropy, etc.) was investigated. Because of its poor speed and significant memory usage, 3D numerical method cannot be used for the inversion and evaluation of dielectric logging data. [1] treated the tool pad as a semi-infinite thick media, developed a simpler model, and combined finite element and analytical solutions to solve the wave equation. The influence of the mud cake was simulated, and the detection performance of the tool was evaluated. This equivalent calculation model substantially simplifies the measurement process while also increasing computation efficiency. It has high applicability for high-frequency (GHz) detection modes but has huge inaccuracies and limited usefulness for lower frequency circumstances. When processing multi-frequency array dielectric logging data, [2, 4] considered the tool pad as an eccentric cylindrical metal mandrel, the antenna as a magnetic dipole, and the formation as a one-dimension (1D) cylindrical layered model. This problem has a semi-analytical solution [10, 11, 17]. The analytical method's great efficiency makes it ideal for the fast forward modeling of dielectric logging.

As a result, based on the push-against scheme of ADT's formation model, this paper derives the semi-analytical expression of magnetic dipole based on a simplified model, proposes a simplified acceleration method, then develops a fast forward calculation algorithm for dielectric logging and discusses its feasibility and applicability. Calibration charts for amplitude attenuation and phase shift with resistivity and permittivity are produced for several dielectric logging measurement modes, and the influence of mud cake, invasion, and anisotropy on signals in different operation modes is simulated.

2. THEORY OF FAST FORWARD SIMULATION METHOD FOR ADT MEASUREMENTS

The Dielectric Scanner is measured by pushing against the borehole wall. It employs multi-frequencies from 20 MHz to 1 GHz, with a maximum antenna distance of 25 cm. It can be noticed that the influence of the bed boundaries can be ignored when the tool is significantly shorter than the thickness of the formation, and the formation environment can be simplified into a 1D radial layered media by replacing the tool pad with a metal cylinder, as shown in Figure 1.

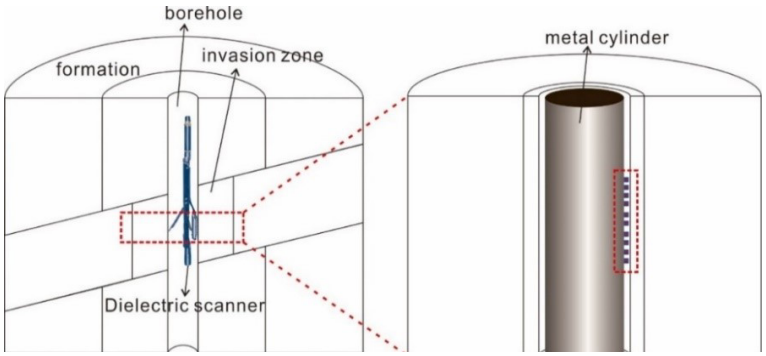

Figure 1. Simplified model for dielectric logging.

Time convention $e^{-i\omega t}$ is implied, and the antenna is regarded as a magnetic dipole (MD) located at the surface of the mandrel. The complex permittivity of formation can be expressed as

$$\hat{\boldsymbol{\varepsilon}}^* = \begin{pmatrix} \varepsilon_h + i\sigma_h/\omega & 0 & 0 \\ 0 & \varepsilon_h + i\sigma_h/\omega & 0 \\ 0 & 0 & \varepsilon_v + i\sigma_v/\omega \end{pmatrix} \tag{1}$$

Maxwell equations can be written as

$$\begin{aligned} \nabla \times \mathbf{H} &= \omega \hat{\boldsymbol{\varepsilon}}^* \mathbf{E} \\ \nabla \times \mathbf{E} &= i\omega\mu \mathbf{H}(\mathbf{r}) + i\omega\mu \mathbf{M}(\mathbf{r}) \end{aligned} \tag{2}$$

Taking the zz component as an example, it can be expressed as Equation (3) based on the rotational symmetry and the invariance of the vertical properties of the formation.

$$\begin{pmatrix} E_{zz} \\ H_{zz} \end{pmatrix} = \sum_{\nu=-\infty}^{\infty} e^{i\nu\varphi} \int_{-\infty}^{\infty} e^{ik_z z} \begin{pmatrix} e_{zz\nu} \\ h_{zz\nu} \end{pmatrix} dk_z \tag{3}$$

where v is the azimuth mode number. The analytical formula of the spectral domain field includes Bessel and Hankel functions, which suffer from the numerical overflow problem due to the high conductivity of metal mandrel in high frequency. In this algorithm, the overflow problem is solved by expressing formulas by the ratios of Bessel or Hankel functions. This makes the algorithm stable at a wide range of frequencies and conductivities [5, 6]. However, when the magnetic dipole is put close to the interface with great resistivity contrast, the truncation number for v becomes much larger. Given that

$$\begin{pmatrix} E_{zz\nu} \\ H_{zz\nu} \end{pmatrix} = \int_{-\infty}^{\infty} \begin{pmatrix} e_{zz\nu} \\ h_{zz\nu} \end{pmatrix} e^{ik_z z} dk_z \tag{4}$$

Since the tool and well axes are parallel, let $\varphi = 0$, and Equation (3) can be expressed as

$$H_{zz} = \tau \sum_{\nu=0}^{\infty} H_{zzv} \tag{5}$$

where $\tau = 1$ if $v = 0$, otherwise, $\tau = 2$.

Set the truncating value of the Fourier modes of Equation (5) as N. Figure 2 shows the absolute value of the imaginary component of $Hzzv$ in logarithmic scale as a function of v with various frequencies and tools positions, where $R = 10\,\Omega\cdot\mathrm{m}$, $\varepsilon_r = 1$, $r_{bh} = 0.1\,\mathrm{m}$. N grows dramatically as MD moves closer to the mandrel's interface, and N also increases as the frequency rises. It can be noticed that when v is bigger than 45, the result is distorted at a frequency equal to 1G. This is because when the MD is attached to a high discontinuous interface under high-frequency conditions, the numerical calculation of the high-order Bessel function becomes unstable. This part should be ignored, and $N = 45$ is a better choice because the value of $|Hzzv|$ is relatively small in comparison to the first few components. When $N < 45$, based on the regularity of $|Hzzv|$ variation, this paper introduces a logarithmic interpolation method to reduce the number of Fourier modes required for calculation and increase the calculation speed of dielectric logging response, given by

$$\begin{aligned} H_{zzv} &= 10^{\log_{10} H_{zzv}} = 10^{f_v} \\ f_v &= P_p(v) + e_p(v) \end{aligned} \tag{6}$$

where $p = v_i - v_{i-1}$, it means to compute Fourier mode once in every p mode. $P_p(v)$ is the polynomial interpolant, and $e_p(v)$ is the error function. A local error function is defined as [15, 16]:

$$Loc_{err}(v) = \left| \frac{\hat{H}_{zzv}}{Hzz}(1/10^{e_p(v)} - 1) \right| \tag{7}$$

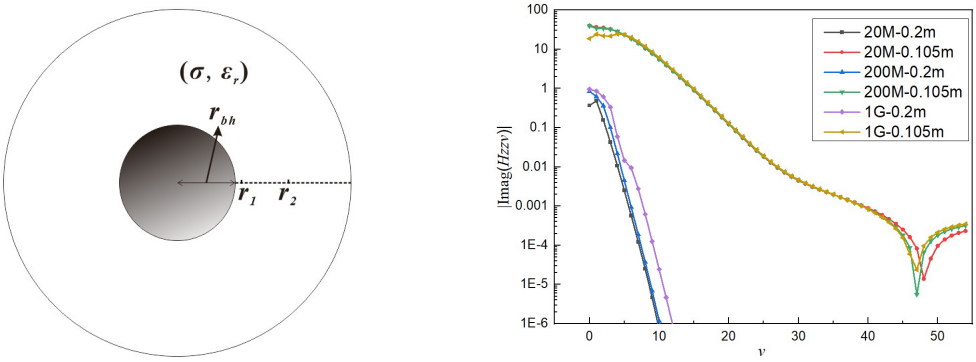

Figure 2. |Imag($Hzzv$)| in logarithmic scale, while the MD is located at $r_1 = 0.105\,\mathrm{m}$ and $r_2 = 0.2\,\mathrm{m}$ under 20 MHz, 200 MHz, and 1 GHz.

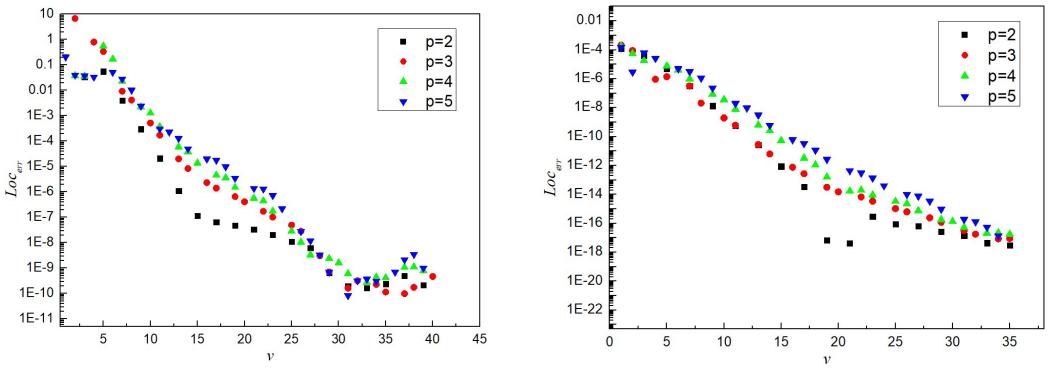

Figure 3. Local error with p ranging from 2 to 5, (a) 1 GHz, (b) 20 MHz.

Figure 3 shows that when v is less than 10, the inaccuracy increases when the interpolation method is used, and it is related to the severe change of the first few harmonic components. The needed calculating Fourier modes can be minimized by using logarithmic interpolation after $v > 10$. For example, under the condition of 1 GHz, $N = 40$, the interpolation interval is $p = 3$, which can save 50% of the total computation.

To verify the accuracy of the algorithm and to study the feasibility of the simplified model, as shown in Figure 4, a centered metal cylinder equivalent model and an eccentric metal cylinder equivalent model are created for comparison [2, 4]. Assume that the wellbore radius $r_{bh} = 0.1$ m, and $(R, \varepsilon_r)_{mud} = (1, 20)$, $(R, \varepsilon_r)_{formation} = (10, 1)$, the results of the algorithm in this paper are compared with that of COMSOL, as shown in Figure 5. The imaginary parts of H_{zz} as a function of source space ranging from 0.0381 to 0.1143 m are obtained. Results show that the algorithm in this paper is validated with COMSOL based on a centered metal cylinder model. There is a slight difference compared to the results of an eccentric cylinder model, and the difference grows as the source space grows larger. The highest difference is roughly 10%, and the difference is smaller at 1 GHz. Though the results of the eccentric metal cylinder model do not represent a real response with the actual tool pad, it can be inferred that the algorithm in this paper is more suitable for the detection mode with high operation frequency and small source spacing. Considering that the centered cylindrical model is more computationally efficient than the eccentric one, the equivalent model algorithm in this paper is highly feasible in dielectric logging.

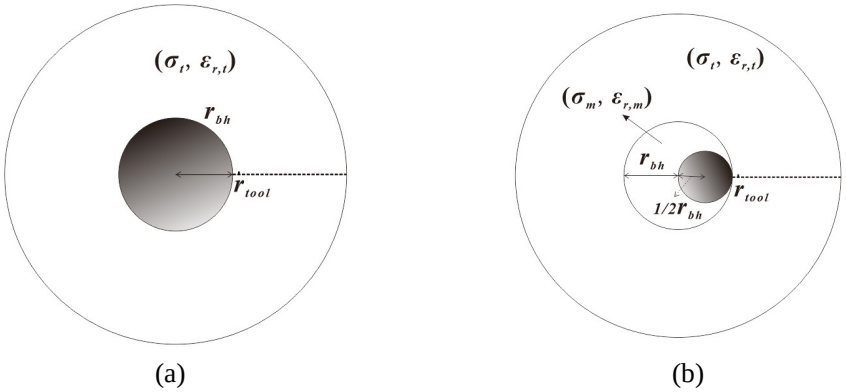

Figure 4. Equivalent computational model of dielectric logging, (a) centered mandrel, (b) eccentric mandrel.

As shown in Figure 6, the ADT uses symmetrically distributed two-transmitting and eight-receiving coils, and this figure depicts the spacing of each coil. Each group coil includes two horizontal and vertical coils. To take the zz component as an example in this paper, as shown in the right of Figure 6, the

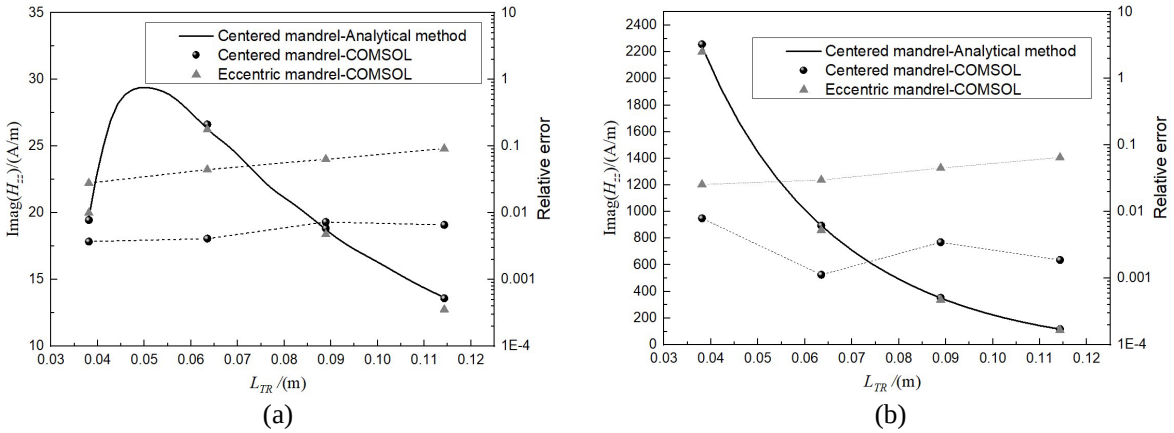

Figure 5. Imaginary part of H_{zz} in the left vertical axis and the relative error in the right vertical axis, as a function of source spacing L_{TR}, (a) 20 MHz, (b) 1 GHz.

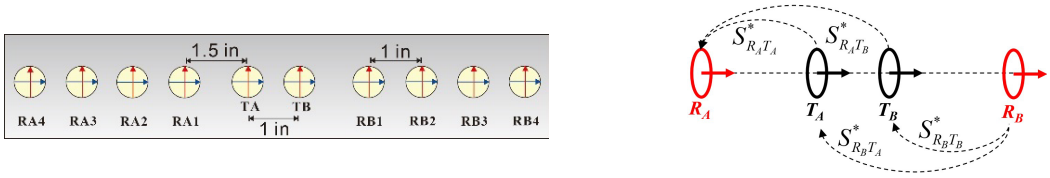

Figure 6. Coil configuration of ADT.

dielectric logging response is calibrated by the amplitude attenuation (Att) and phase shift (PS), as shown in Equation (8).

$$\begin{aligned} Att &= \frac{1}{2}(Att_A + Att_B) & PS &= \frac{1}{2}i(\Delta\phi_A + \Delta\phi_B) \\ Att_A &= 20\log_{10}\left(\mathrm{abs}(S^*_{R_AT_A})/\mathrm{abs}(S^*_{R_AT_B})\right) & \Delta\phi_A &= \arg(S^*_{R_AT_A}) - \arg(S^*_{R_AT_B}) \\ Att_B &= 20\log_{10}\left(\mathrm{abs}(S^*_{R_BT_B})/\mathrm{abs}(S^*_{R_BT_A})\right) & \Delta\phi_B &= \arg(S^*_{R_BT_B}) - \arg(S^*_{R_BT_A}) \end{aligned} \tag{8}$$

We must calculate the zz or xx field 128 times from the two-transmitting and eight-receiving coil system at four operating frequencies for each ADT logging point. It is time-consuming work. Therefore, according to the invariance of the longitudinal properties of the equivalent cylindrical layered model, we need to only compute 5 responses with varied source spacing instead of 16 for the permutations of double-transmitting and eight-retracting coil, because only 5 alternative source spacings exist. Then, it can be noticed that the spectral domain fields e_{zzv} and h_{zzv} in Equation (3) are independent of z, and the spectral domain field and integration part can be calculated separately, thus a single logging point only needs to calculate the spectral domain field once and then execute five times of integration for different source spacings. Calculating 10 logging points of distinct formation models with a single frequency on a computer with a 9th generation Intel i7 CPU, for example, takes the time stated in Table 1. The algorithm in this study may improve the calculation efficiency of the ADT response of a single measurement point by more than 8 times, as shown in the table.

3. RESPONSE CHARACTERISTICS OF ADT

The Att and PS are simulated at different frequencies to evaluate the influence of formation resistivity and permittivity on the dielectric logging response, as illustrated in Figure 7. The PS is calibrated between -180 degrees and 180 degrees, and the formation resistivity ranges from 1 to 500 $\Omega\cdot$m, while relative permittivity ranges from 1 to 100. Comparing to each other, the Att and PS corresponding to the four frequencies are notably different. The PS does not reflect relative permittivity and is sensitive

Table 1. Acceleration method of ADT response.

Methods	without acceleration (50 times calculation)	Logarithmic interpolation ($p = 2$)	Logarithmic interpolation ($p = 3$)	spectral field separation calculation ($p = 3$)
Time(s)	13.53	8.63	6.83	1.58

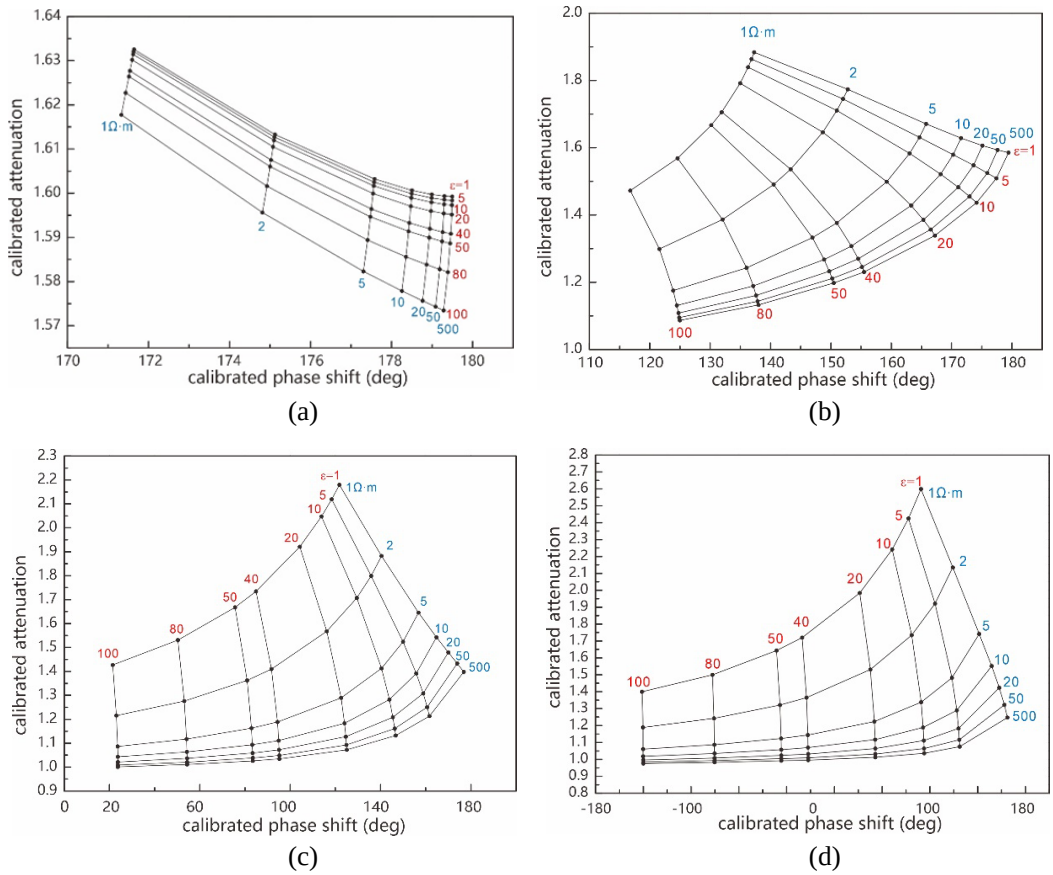

Figure 7. Calibrating charts of Dielectric Logging response, (a) 20 MHz, (b) 200 MHz, (c) 500 MHz, (d) 1 GHz.

to resistivity at 20 MHz because the relative permittivity curve at a fixed resistivity is approximately parallel to the vertical axis. The *PS* value, however, does not vary significantly, ranging from 170 to 180 degrees, and the *Att* changes are less than 0.1, with resistivity ranging from 1 to 500 $\Omega \cdot$ m, because of the low frequency and close distance between the two transmitters, and extracting the corresponding formation parameters is challenging. The relative permittivity curve for a given resistivity shifts to the horizontal axis as the frequency rises, implying that the PS is more sensitive to relative permittivity at high frequencies, and it is more obvious in resistive formation. In the figure of 1 GHz, when the resistivity is greater than 20, the permittivity curve at a fixed resistivity is parallel to the horizontal axis, and it is beneficial to accurately extract the permittivity. Generally, low frequency is more favorable for resistivity, but due to the small spacing of the transmitting coils, there exists only a weak signal difference at low frequency. It is generally difficult to determine the resistivity of the high-resistive formation under a single frequency, and it is necessary to combine the other frequency modes to jointly

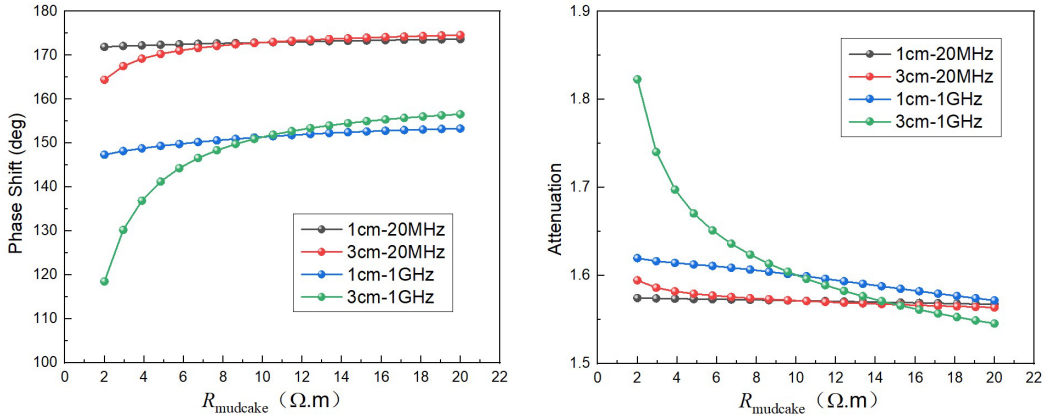

Figure 8. Dielectric logging response, *PS* is shown at the left figure and *Att* at the right figure, as a function of mud cake resistivity, two thicknesses of mud cake under two frequencies are shown in figure.

determine the resistivity of the resistive formation. The calibration accuracy of formation resistivity decreases with the increase of resistivity and relative permittivity, while it is more accurate to extract relative permittivity at resistive formation.

Dielectric logging mainly detects mud cakes and invasion zones around the well. First, mud cake models with thicknesses of 1 cm and 3 cm are constructed. The borehole radius is $r_{bh} = 0.1$ m, and (R_h,

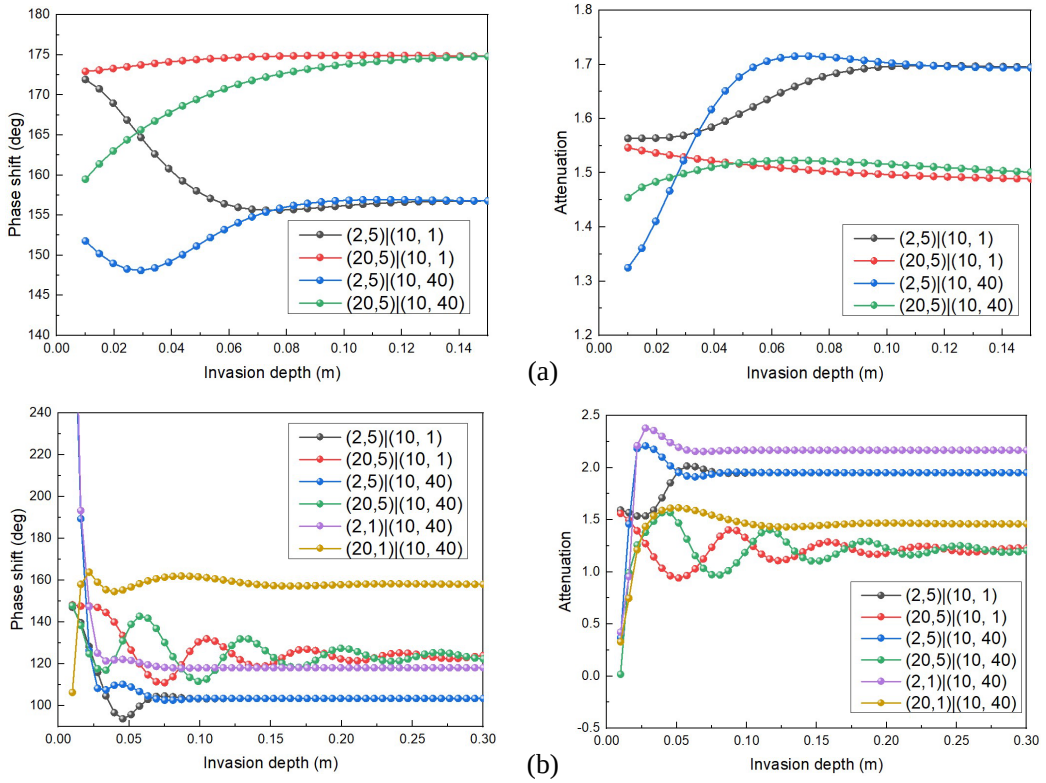

Figure 9. Dielectric logging response, *PS* is shown at the left figure and *Att* at the right figure, as a function of invasion depth, (2, 5)|(10, 1) means an invasion zone with resistivity $= 2\,\Omega\cdot$m and relative permittivity $= 5$ and a formation with resistivity $= 10\,\Omega\cdot$m and relative permittivity $= 1$, (a) 200 MHz, (b) 1 GHz.

$\varepsilon_r)_{formation} = (10, 1)$. As shown in Figure 8, its response changes as a function of mud cake resistivity at different frequencies. When the thickness of the mud cake is 3 cm, the high-frequency response is greatly affected by the mud cake, and the lower the resistivity of the mud cake is, the greater the response change is. The mud cake is unaffected when the size of the mud cake is 1 cm. It can be inferred that the extraction of mud cake parameters by high-frequency detection mode is a good way.

To study the influence of the invasion zone on the response, the resistivity of the intrusion zone was set as $2\,\Omega\cdot$m and $20\,\Omega\cdot$m, and the relative permittivity was set as 10. The *PS* and *Att* as a function of invasion depth are shown in Figure 9. The depth of investigation in this detection mode can be roughly judged by the change of invasion depth as the responses are not sensitive to formation when the curve goes flat. For example, under the condition of 20 MHz, the *PS* signal does not change when the invasion is about 8 cm, while the *Att* signal tends to remain unchanged when it is above 10 cm, indicating that the depth of investigation of the *PS* signal is smaller than that of the *Att* signal. When the relative permittivity of the formation is larger, it can be seen that the sensitivity range goes deeper, and it is especially obvious at 1 GHz, as shown in the third and fourth graphs of Figure 9. It is worth noting that increasing the invasion zone's resistivity or permittivity can easily cause the response to oscillate as a function of invasion depth. As the high-frequency and high-resistivity conditions will improve the contribution of the permittivity to the response, it indicates that the high-frequency detection mode exhibits higher sensitivity and deeper depth of investigation for high-resistivity and high-permittivity formations.

Let the horizontal resistivity of the formation be 1, 2, and $5\,\Omega\cdot$m and the resistivity anisotropy coefficient $\lambda = \sqrt{R_v/R_h}$, to simulate the *PS* and *Att* response of the *xx* component as a function of formation resistivity anisotropy, as shown in Figure 10, it reveals that at 20 MHz, the *PS* and *Att* of low-resistivity formations are more sensitive to resistivity anisotropy, whereas formation permittivity

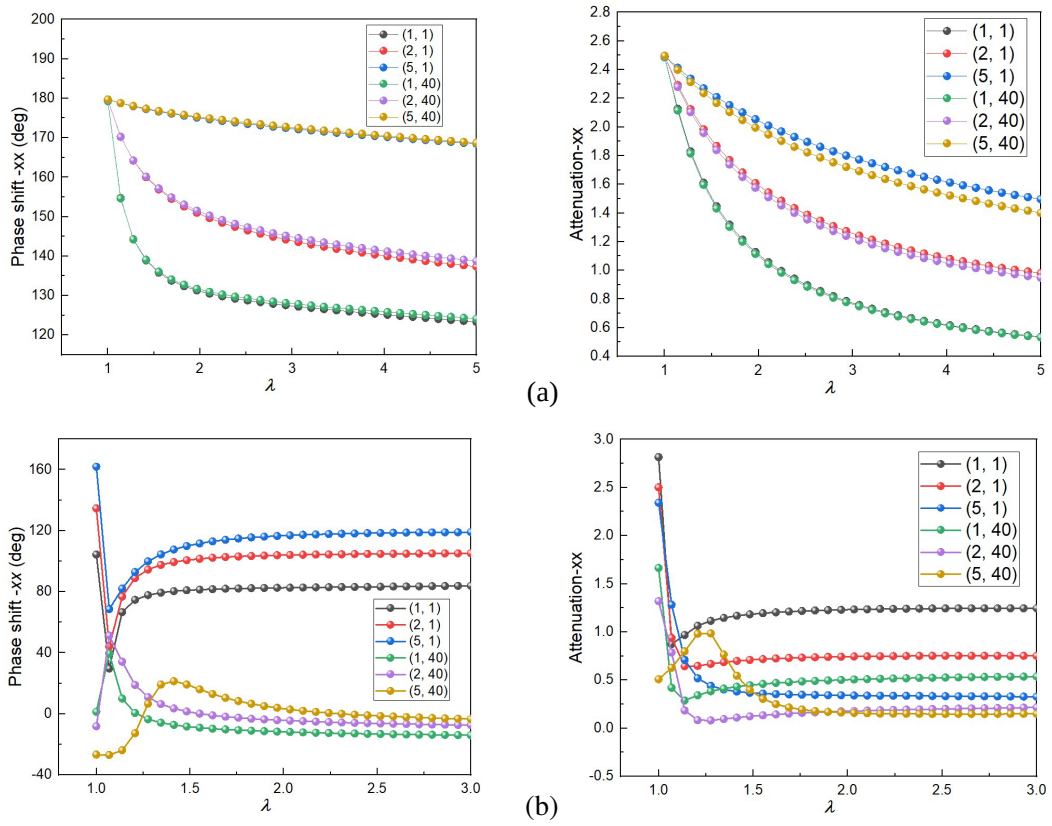

Figure 10. Dielectric response of *xx* component, *PS* is shown at the left figure and *Att* at the right figure, as a function of formation resistivity anisotropy, with different formation horizontal resistivity and relative permittivity.

has no effect. When the anisotropy coefficient becomes larger, the sensitivity of *Att* to anisotropy is higher than that of *PS*. Under the frequency of 1 GHz, the response changes sharply when λ is small, indicating high sensitivity, when $\lambda > 2$; however, the curve becomes flat and is no longer sensitive to anisotropy. Furthermore, the formation permittivity has a significant impact because the curve splits significantly at different relative permittivities, particularly for the *PS* signal.

4. CONCLUSION

In this paper, a simplified calculation model of ADT is established, and a stable algorithm based on the semi-analytical formula for dielectric logging is developed. By introducing the logarithmic interpolation approach for calculating harmonic components and providing a spectral-domain separation computation procedure, the response time for a single measurement point has been increased by more than 8 times. And the algorithm's applicability to dielectric logging at high frequency and short source spacing is determined through comparison and testing. It establishes the groundwork for dielectric recording data processing. Through numerical simulation, we arrive at the following conclusions:

(1) It can be seen that the high-frequency response changes significantly when the mud cake is thick, and the mud cake parameters can be extracted by the high-frequency detection mode.

(2) The high-frequency dielectric logging response is complex, and an increase in the invasion zone's resistivity or relative permittivity can easily lead to an oscillatory nonlinear change in the response. This indicates that the high-frequency dielectric detection mode has higher sensitivity and deeper detection depth for formations with high resistivity and permittivity.

(3) When the anisotropy coefficient is modest, the high-frequency response is useful for extracting anisotropy; however, as the anisotropy rises, the low-frequency response becomes more sensitive to anisotropy than the high-frequency response. At the same condition, the *Att* has a larger sensitivity to anisotropy than the *PS*, and the response is more susceptible to anisotropy at low-resistivity formation.

ACKNOWLEDGMENT

The authors are indebted to the financial support from the Natural Science Foundation of China (41674131, 41574118), the Major Scientific and Technological Projects of China National Petroleum Corporation (ZD2019-184-001-002), and the Postgraduate Innovation Fund Project of China University of Petroleum (YCX2021003).

REFERENCES

1. Chew, W. C., "Modeling of the dielectric logging tool at high frequencies: Applications and results," *IEEE Transactions on Geoscience and Remote Sensing*, Vol. 26, No. 4, 388–398, 1988, https://doi.org/10.1109/36.3042.
2. Forgang, S., B. Corley, A. Garcia, A. Hanif, F. Le, J. Jones, et al., "A new multi-frequency array-dielectric logging service: Tool physics, field testing, and case studies in the permian basin wolfcamp shale," *SPWLA 60th Annual Logging Symposium Transactions*, 1–21, Society of Petrophysicists and Well Log Analysts, 2019, https://doi.org/10.30632/T60ALS-2019_W.
3. Herlinger, R., "Dielectric logging: Principles, applications, and examples from the Brazilian oilfields," *Offshore Technology Conference Brasil 2019, OTCB 2019*, 2020, https://doi.org/10.4043/29882-ms.
4. Hizem, M., H. Budan, B. Deville, O. Faivre, L. Mosse, and M. Simon, "Dielectric dispersion: A new wireline petrophysical measurement," *SPE Annual Technical Conference and Exhibition*, Society of Petroleum Engineers, Denver, Colorado, USA, 2008, https://doi.org/10.2118/116130-MS.
5. Hong, D., W.-F. Huang, and Q. H. Liu, "Radiation of arbitrary magnetic dipoles in a cylindrically layered anisotropic medium for well-logging applications," *IEEE Transactions on Geoscience and Remote Sensing*, Vol. 54, No. 11, 6362–6370, 2016, https://doi.org/10.1109/TGRS.2016.2582535.

6. Hong, D., W.-F. Huang, H. Chen, and Q. H. Liu, "Novel and stable formulations for the response of horizontal-coil eccentric antennas in a cylindrically multilayered medium," *IEEE Transactions on Antennas and Propagation*, Vol. 65, No. 4, 1967–1977, 2017, https://doi.org/10.1109/TAP.2017.2670360.
7. Kang, Z., S. Ke, C. Yin, W. Wang, S. Zheng, X. Sun, and J. Li, "Dielectric constant measurements of sweep frequency and its effect from 20 MHz to 1000 MHz," *Journal of Petroleum Science and Engineering*, Vol. 166, 602–610, March 2018, https://doi.org/10.1016/j.petrol.2018.03.093.
8. Little, J. D., D. R. Julander, L. C. Knauer, J. T. Aultman, and J. L. Hemingway, "Dielectric dispersion measurements in California heavy oil reservoirs," *SPWLA 51st Annual Logging Symposium*, SPWLA-2010-14021, Society of Petrophysicists and Well-Log Analysts, Perth, Australia, 2010.
9. Liu, C. R., "Principle of dielectric logging tools," *Theory of Electromagnetic Well Logging*, 447–501, Elsevier, 2017, https://doi.org/10.1016/B978-0-12-804008-9.00012-1.
10. Liu, H., D. Hong, N. Li, W. Han, and Q. H. Liu, "Solving electromagnetic fields by general reflection\transmission method for coaxial-coil antenna in cylindrically multilayered medium," *IEEE Geoscience and Remote Sensing Letters*, Vol. 15, No. 6, 912–916, 2018, https://doi.org/10.1109/LGRS.2018.2814614.
11. Lovell, J. and W. Chew, "Response of a point source in a multicylindrcally layered medium," *IEEE Transactions on Geoscience and Remote Sensing*, Vol. 25, No. 6, 850–858, 1987, https://doi.org/10.1109/TGRS.1987.289757.
12. Mosse, L., R. Carmona, E. Decoster, O. Faivre, and M. Hizem, "Dielectric dispersion logging in heavy oil: A case study from the orinoco belt," *SPWLA 50th Annual Logging Symposium*, 16, Society of Petrophysicists and Well-Log Analysts, The Woodlands, Texas, 2009.
13. Pirrone, M., H. Mei, N. Bona, M. Borghi, M. T. Galli, F. Pampuri, et al., "A novel approach based on dielectric dispersion measurements to evaluate the quality of complex shaly-sand reservoirs," *SPE Annual Technical Conference and Exhibition*, 13, Society of Petroleum Engineers, Denver, Colorado, USA, 2011, https://doi.org/10.2118/147245-MS.
14. Rabinovich, M., S. Liu, F. Le, H. M. Maurer, and J. Dahl, "Challenges of measuring dielectric anisotropy with high-frequency dielectric logging tools," *SPWLA 56th Annual Logging Symposium 2015*, SPWLA-2015-JJ, 2015.
15. Rodríguez-Rozas, Á. and D. Pardo, "A priori fourier analysis for 2.5D finite elements simulations of logging-while-drilling (LWD) resistivity measurements," *Procedia Computer Science*, Vol. 80, 782–791, 2016, https://doi.org/10.1016/j.procs.2016.05.368.
16. Rodríguez-Rozas, Á., D. Pardo, and C. Torres-Verdín, "Fast 2.5D finite element simulations of borehole resistivity measurements," *Computational Geosciences*, Vol. 22, No. 5, 1271–1281, 2018, https://doi.org/10.1007/s10596-018-9751-7.
17. Rosa, G. S. and J. R. Bergmann, "Pseudo-analytical modeling for the electromagnetic propagation in stratified cylindrical structures," *IEEE Antennas and Wireless Propagation Letters*, Vol. 15, 344–347, 2016, https://doi.org/10.1109/LAWP.2015.2444418.
18. Seleznev, N. V., R. L. Kleinberg, M. M. Herron, M. Machlus, A. E. Pomerantz, S. L. Reeder, et al., "Applications of dielectric dispersion logging to oil shale reservoirs," *SPWLA 52nd Annual Logging Symposium*, SPWLA-2011-G, Society of Petrophysicists and Well-Log Analysts, Colorado Springs, Colorado, 2011.